MSDE

PAPER

View Article Online
View Journal

Cite this: DOI: 10.1039/d6me00057f

Conformational behaviour of photoresponsive single-chain polymeric nanoparticles

Tessa Loman, Yagmur Altunsoy, Andra-Maria Olaru, Harshit Singh, A. J. H. Spiering and Anja R. A. Palmans *

Inspired by nature's dynamic materials, we here develop photoresponsive single-chain polymeric nanoparticles (SCPNs) that undergo light-induced changes in their polymeric microenvironment while retaining their global conformation. Stimuli-responsive SCPNs have been explored, but stable photoswitches that operate through solubility switching in water remain underdeveloped. We investigate water-soluble SCPNs with three different covalently attached photoswitches that are based on donor–acceptor Stenhouse adducts (DASAs), spiropyran, or the aryl azopyrazolium ionic photoswitch (AAIP). From the photophysical studies, we identify AAIP as the most robust photoswitch, displaying excellent photostability, high photostationary-state fidelity, and minimal fatigue. Using dynamic light scattering (DLS), fluorescence probes, nuclear magnetic resonance (NMR), and small angle X-ray (SAXS) studies, we elucidate how photoswitching and side-graft design affect the global SCPN conformation. SAXS reveals compact nanoparticles ($R_G \approx 5$–6 nm) for all AAIP functionalized polymers, and their global conformation is not affected by the *E*–*Z* photoisomerization of the AAIP grafts. In contrast, NMR and fluorescence data indicate a clear shift in microenvironment polarity upon photoisomerization. In addition, cytotoxicity assays show that the biological response is highly sensitive to subtle structural variations within these polymers. Together, these findings expand our knowledge of light-responsive SCPNs by introducing a new, stable photoswitch. Our results demonstrate that local microstructure and global conformation can be decoupled, and highlight the importance of precise polymer design for future biological applications.

Received 20th March 2026,
Accepted 4th May 2026

DOI: 10.1039/d6me00057f

rsc.li/molecular-engineering

Design, System, Application

Nature provides ample examples of dynamic materials in which stimuli-responsive motifs are paramount to their adaptive functions, inspiring efforts to translate such behaviour into synthetic systems. Light is a particularly attractive stimulus due to its precise temporal and spatial controllability and its clean and non-invasive nature. In single-chain polymeric nanoparticles (SCPNs), light-responsiveness has predominantly been engineered through covalent photochemistry, leaving the potential of solubility-switching photoswitches largely unexplored. Therefore, we here introduce light-responsiveness into SPCNs by incorporation of donor–acceptor Stenhouse adducts, spiropyrans and aryl azopyrazolium photoswitches, each of which undergoes photoisomerization to a more hydrophilic state upon irradiation. This strategy enables us to probe how a molecular adjustment in hydrophobicity influences the SCPNs behaviour within their inherently dynamically collapsed conformations. In our strategy we first study the photophysical properties of the photoswitches within the SCPNs, allowing us to identify the most robust and stable system. Further, we disentangle global and local effects by examining the global particle conformation using small-angle X-ray scattering and the polymer microstructure through pyrene fluorescence. Our results demonstrate that local microstructure and global conformation can be decoupled, highlighting that polarity modulation does not necessarily induce large-scale structural reorganization. These insights emphasize the importance of precise polymeric design for future biological applications.

Introduction

Nature provides numerous examples of dynamic and responsive materials, inspiring the development of smarter synthetic systems with enhanced functionalities.[1] Over recent decades, the design of stimuli-responsive materials has emerged as a central theme, leading to systems responsive to diverse triggers, such as pH,[2,3] temperature,[4,5] metal ions,[6,7] small molecules[8,9] and light.[10,11] Among these stimuli, the use of light is particularly attractive due to its precise temporal and spatial controllability and its clean and non-invasive nature. Furthermore, when operating in the visible range, it is largely non-destructive. Consequently, light-responsive moieties, photoswitches, have been widely integrated into functional materials.

A broad variety of photoswitches are available, including azobenzenes,[12] spiropyrans[13] and donor–acceptor Stenhouse

Department of Chemical Engineering & Chemistry and Institute for Complex Molecular Systems, Eindhoven University of Technology, P.O. Box 513, 5600 MBEindhoven, The Netherlands. E-mail: a.palmans@tue.nl

adducts (DASAs).[14] Although their photochemical mechanisms differ, photoisomerization in each case typically introduces changes in polarity, hydrophilicity and molecular geometry. In aqueous environments, these changes provide a means to modulate solubility, interactions and assemblies of synthetic systems.

Azobenzenes represent one of the most extensively studied classes of photoswitches.[15,16] Upon UV irradiation they undergo an isomerization from the stable *E* to metastable *Z*-isomer. The metastable *Z*-isomer subsequently isomerizes back to the *E*-isomer, a process which can be accelerated using light of a specific wavelength. The dipole moment of the *Z*-isomer is significantly larger than that of the *E*-isomer, resulting in the *Z*-isomer being more polar and hydrophilic.[17] Classical azobenzenes exhibit excellent photostability with minimal fatigue, yet they are challenged by relatively short *Z*-isomer lifetimes and limited water solubility.[18] These drawbacks have led to the development of heteroaryl azo dyes such as aryl azopyrazoles.[19] Recent work by Venkataramani and coworkers further advanced this class by quarternizing the pyrazole ring, yielding aryl azopyrazolium ionic photoswitches (AAIP) with enhanced water solubility, excellent switching performance, and markedly slower thermal relaxation.[20]

To the best of our knowledge, AAIPs have not yet been applied to control conformational changes within macromolecular systems. In contrast, aryl azopyrazoles have been successfully used to modulate the conformation of well-designed architectures. For example, Manna *et al.* incorporated aryl azopyrazole side chains into a poly(ethylene glycol methacrylate)-*b*-poly(aryl azopyrazole methacrylate) copolymer, demonstrating that photoinduced *E–Z* isomerization leads to a pronounced deformation of spherical polymeric micelles.[21] Furthermore, Laschewsky and coworkers employed an aryl azopyrazole moiety to impart thermo- and photoresponsive behaviour to water-soluble acrylamide copolymers, enabling reversible tuning of the LCST phase transition through *E–Z* isomerization.[22]

In contrast to the *E–Z* isomerization of azobenzene derivatives, spiropyrans shift between a neutral hydrophobic spiropyran (SP) isomer and a highly polar zwitterionic merocyanine (MC) isomer. This isomerization is accompanied by a substantial increase in dipole moment and a corresponding decrease in hydrophobicity.[13,23] These properties have been exploited to modulate hydrophilicity in soft materials, for example in hydrogels, as demonstrated by Li *et al.*[24] Kohane and coworkers further used spiropyrans to control nanoparticle conformation, observing reversible size changes from 150 to 40 nm upon photoisomerization.[25] Furthermore, spiropyran functionalized hyperbranched polyglycerols were engineered to regulate polymer micelle assembly and disassembly *via* the photoisomerization process.[26]

Both azobenzenes and spiropyrans typically require UV light for activation. To enhance tissue penetration and hereby reduce potential phototoxicity effects in biological application, Read de Alaniz and coworkers applied DASAs, which respond to visible light.[27] DASAs consist of a donor–acceptor framework connected by a triene bridge, enabling reversible switching between the elongated, strongly coloured triene isomer and the colourless, polar cyclopentenone isomer. This loss of color, named negative photochromism, improves light penetration by reducing absorption in already activated regions. Moreover, the isomerization is accompanied by a significant difference in solubility parameters.[28] These characteristics have been employed in a micellar drug delivery vehicle, showing the potential of DASA in biomedical applications.[29] Additionally, DASA incorporation was used to tune the permeability of polymersome membranes, leading to control over substrate diffusion.[30]

Inspired by these examples, we introduce photo-responsiveness into single-chain polymeric nanoparticles (SCPNs) by introducing DASA, spiropyran or AAIP grafts. SCPNs are widely studied and show promising applications in biosensing,[31] drug delivery[32,33] and green[34,35] and bio-orthogonal catalysis.[36] SCPNs form by the spontaneous collapse/folding of a single, amphiphilic heterograft polymeric chain in water, creating a nanoparticle with protein-like characteristics.[37,38] This collapse can be driven by covalent crosslinking,[39] H-bonding units,[40,41] metal coordination[42,43] or hydrophobic effects.[44] Interestingly, light-responsive crosslinking strategies have been reported as a means to control chain conformation of SCPNs. Our group has shown that coumarin photo-dimerization enables pathway-dependent SCPN morphologies, obtaining control over the compactness and size of the resulting SCPNs.[45] Building on this concept, the crosslinking and fluorescence reporting function was unified in one motif using the nitrile imine-mediated tetrazole–ene cycloaddition (NITEC) reaction.[46] Similarly, Barner-Kowollik and coworkers used the metal coordinating functionality of a spiropyran functionalized PEGMEMA to induce a light-triggered collapse of the polymeric chain.[47]

In the present study, we use SCPNs comprising a random heterograft amphiphilic polymer relying on the hydrophobic effect for particle formation (Scheme 1). Herein, the hydrophobic side-grafts drive the collapse of the polymeric chain, while hydrophilic side-grafts ensure the water solubility of the nanoparticle. As the solubility characteristics of photoswitches vary greatly between photoisomers, grafting such moieties covalently onto the amphiphilic polymeric backbone is expected to influence the SCPN morphology in aqueous environments. We therefore investigate the influence of DASA, spiropyran and AAIP photoswitches on SCPN morphology. We further explore how the photoisomerization process modulates the SCPN conformation and assess how this impacts the biological applicability of the resulting systems.

Results and discussion

Polymeric design and synthesis

To study the influence of covalent side-grafting of photoresponsive moieties on SCPNs, we designed a series

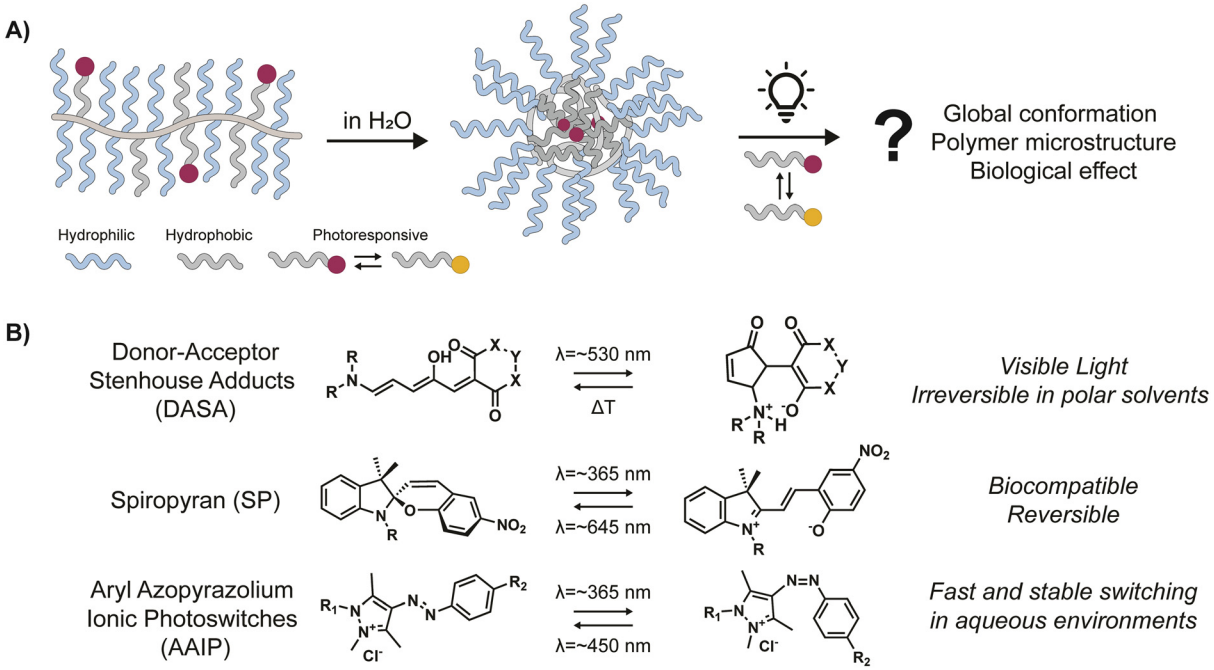

Scheme 1 A) Visual representation of a random heterograft amphiphilic polymer decorated with a photoresponsive motif and its collapse in aqueous environments. B) General structures of common photoswitches DASA, SP and AAIP and their characteristics.

of random heterograft polymers inspired by architectures previously developed in our group.[48] By systematically varying the photoswitch, hydrophilic component and overall composition, we create distinct polymer microstructures that enable us to probe the photoisomerization effects across multiple polymeric environments. The compositions of the photoresponsive polymers **P1–P5** are summarized in Table 1.

P1–P5 were synthesized analogous to the previously reported post-functionalization approach (synthetic details in SI).[49] First, a RAFT-polymerized poly(pentafluorophenyl acrylate) homopolymer (pPFPA) was synthesized, which was subsequently decorated with *n*-dodecylamine side-grafts to induce hydrophobic collapse and either Jeffamine M1000 or glucosamine to impart water solubility. Propargylamine was introduced as an additional graft to function as click-handle for the later photoswitch addition (Chart 1). Several polymer compositions were designed. For Jeffamine M1000-decorated SCPNs, 80 mol% Jeffamine, 10 mol% *n*-dodecylamine and 10 mol% propargylamine were used. These ratios were chosen based on prior work showing that 20 mol% *n*-dodecylamine and 80 mol% Jeffamine M1000 resulted in well-collapsed particles.[50] In addition, the amount of functional alkyne was kept below 10 mol% as we anticipated that a higher amount of photoswitch (see below) may lead to changes in global conformation due to charge repulsion[51] or lead to cytotoxicity effects in cellular media.[52] For glucose-based SCPNs **P4** and **P5**, the hydrophilic content was slightly increased to 85 mol% to compensate for the

Table 1 Overview of the amphiphilic copolymer composition, theoretical number averaged molecular weight (M_n) and molar mass dispersity ($Đ$) of **P1–P9**

Polymer	x	y	R_1	z	R_2	DP[a]	$M_{n,th}$[b] (kg mol^{-1})	$Đ$[c]
P1	0.10	0.80	Jeff	0.10	DASA	194	186	1.47[d]
P2	0.11	0.82	Jeff	0.07	SP	200	188	1.91[d]
P3	0.10	0.80	Jeff	0.10	AAIP	194	180	1.29[d]
P4	0.10	0.86	Glu	0.04	AAIP	173	42	1.95[e]
P5	0.06	0.86	Glu	0.08	AAIP	173	44	—[f]
P6	0.10	0.86	Glu	0.04	Propargyl	173	40	1.87[e]
P7	0.06	0.86	Glu	0.08	Propargyl	173	44	1.84[e]
P8	0.20	0.80	Jeff	0	—	194	178	1.38[d]
P9	0	1.0	Glu	0	—	173	38	1.36[e]

x, y and z were determined by ^{19}F-NMR. [a] Determined from conversion calculated from ^{19}F-NMR. [b] $M_{n,th}$ was calculated from DP and the composition. [c] $Đ$ was measured by SEC. [d] DMF with 10 mM LiBr, relative to poly(ethylene oxide standards). [e] PBS (pH = 7.4), relative to poly(ethylene oxide standards). [f] Could not be determined.

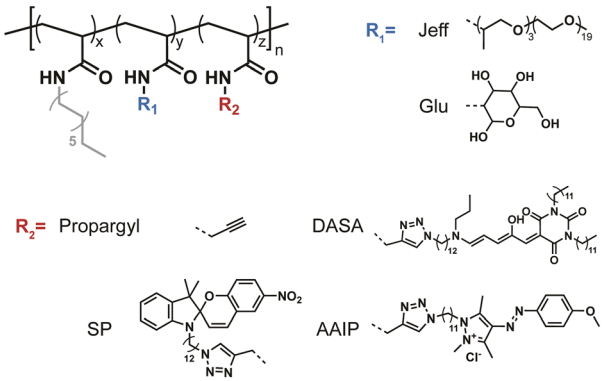

Chart 1 Chemical structures of the studied amphiphilic polymers **P1**–**P9**.

smaller size of the glucose moiety. **P4** and **P5** contain the same monomeric components but differ in their composition. **P4** incorporates 10 mol% *n*-dodecylamine and 5 mol% propargylamine, whereas **P5** contains 5 mol% *n*-dodecylamine and 10 mol% propargylamine, maintaining a constant total hydrophobic content of 15 mol%.

All amphiphilic polymers were subsequently conjugated to a photoswitch – DASA, SP, or AAIP – *via* CuAAC chemistry, yielding polymers **P1**–**P5** (Chart 1, Table 1).[53] The photoswitches were all synthesized following modified literature procedures to include an azide functionality to ensure compatibility with the CuAAC reaction and a C11 or C12 hydrophobic spacer to enhance the hydrophobic effect (synthetic details in SI, Fig. S1–S52).

These synthetic efforts resulted in a focused polymer library. The Jeffamine M1000 decorated polymers **P1**–**P3** bearing the three different photoswitches allow direct comparison of photophysical behaviour. The AAIP functionalized polymers **P3**–**P5** further enable us to examine how polymer microstructure influences photoswitch performance. To support these comparisons, several control polymers were included: **P6** and **P7**, the respective precursors to **P4** and **P5**, contain only the propargyl functionalized backbone; **P8**, comprising 20 mol% *n*-dodecylamine and 80 mol% Jeffamine M1000, represents our established benchmark for Jeffamine M1000 based SCPNs and **P9** is a fully hydrophilic polymer bearing 100 mol% glucose side chains.

All polymers were fully characterized using ^{1}H-NMR and GPC (Table 1, Fig. S53–S83). The successful incorporation of the photoresponsive moieties was confirmed using ^{1}H-NMR, where in all polymers characteristic peaks for the photoswitches were visible, albeit too small to accurately quantify. The efficiency of the CuAAC reaction was therefore quantified *via* UV-absorbance of **P3** and was found to be >95% (Fig. S84). Due to insolubility of the DASA and SP photoswitch in water, this analysis was not performed for **P1** and **P2**, but we assume a similar efficiency.

Photophysical characterization of photoswitch-functionalized polymers

To compare the behaviour of different photoswitches within a consistent polymeric environment, we evaluated the photophysical properties of **P1**–**P3**, in which DASA, SP, and AAIP photoswitches, respectively, are grafted onto the Jeffamine M1000 based SCPN scaffold. This polymer architecture serves as our benchmark for assessing photoswitch performance in aqueous media. First, we assessed the thermal stability of the photoswitches when covalently attached to the SCPN backbone. Especially DASA and SP photoswitches are known to potentially exist in equilibria between their respective isomeric states, depending on the local environment (Fig. 1A).[28] Fig. 1B therefore represents the normalized absorbance at the characteristic wavelength of the more hydrophobic isomer (Fig. 1A), allowing us to monitor thermal isomerization over time. **P1**, containing the DASA photoswitch, exhibits a pronounced decrease in absorbance at 551 nm, corresponding to the open **P1a** isomer. This decline reflects thermal conversion to the zwitterionic **P1b** form, with a measured half-life of 1.3 h. The system ultimately reaches a photostationary state (PSS) with a **P1a**:**P1b** ratio of 38:62. Similarly, **P2** gradually transitions from the closed spiropyran (**P2a**) to the merocyanine (**P2b**) form, evidenced by an increase in absorbance around 550 nm over 15 h (Fig. 1B, S85 and S86). These transitions are also visually apparent: the vibrant purple of isomer **P1a** in **P1** fades over time, while **P2** develops a pink hue indicative of the merocyanine (**P2b**) species.

In contrast, **P3**, functionalized with AAIP, is extremely photostable in its thermodynamically favoured *E*-isomer (**P3a**, Fig. 1A). No significant changes are observed in the absorbance bands at 345 nm (π–π*) and 436 nm (n–π*) over the same time period (Fig. 1B, S87A and B).

Upon irradiation with the appropriate wavelength, **P1**–**P3** all undergo photoisomerization, though with markedly different kinetics (Fig. 1C). **P1** responds slowly to 530 nm light, showing a 90% reduction in the 559 nm absorption band over 120 min (Fig. 1D). Interestingly, partial thermal recovery (~20%) occurs overnight, contrasting with the typical irreversible switching of first-generation DASAs in water (Fig. S88). Similar effects have been observed for sterically congested DASA.[54] **P2** undergoes rapid photoisomerization from **P2a** to **P2b** upon illumination with 365 nm light, reaching maximum absorbance at 551 nm within ~1.5 min (Fig. 1E). However, continued illumination leads to photobleaching, as indicated by the upward trend in Fig. 1C. The merocyanine form also thermally relaxes back to spiropyran with a half-life of 25 min (Fig. S89). **P3** demonstrates the fastest and most robust switching behaviour from **P3a** to **P3b**. *E*–*Z* isomerization occurs within 30 s upon 365 nm light irradiation, with no photobleaching observed (Fig. 1F). The *Z*-isomer (**P3b**)

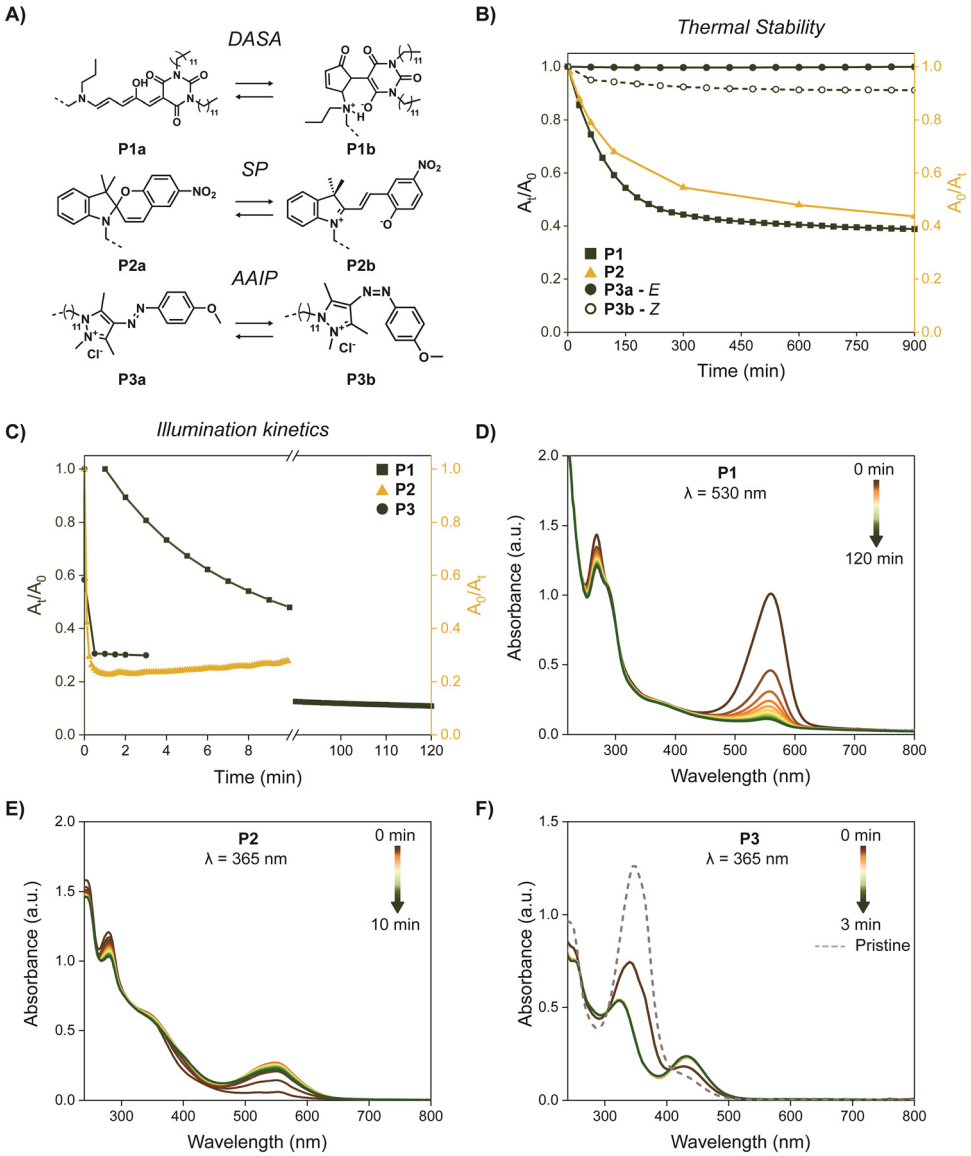

Fig. 1 A) Chemical structures of the photoresponsive side-grafts and their photoisomerization. B) Thermal stability of **P1**–**P3** in Milli-Q under dark conditions. Absorption spectra are evaluated at the absorption maximum with **P1a** at 551 nm, **P2a** at 540 nm, **P3a** at 345 nm and **P3b** at 426 nm. C) Illumination kinetics of **P1**–**P3** in Milli-Q. **P1a** is illuminated with 530 nm light, **P2a** and **P3a** with 365 nm light. **P1a** is evaluated at 559 nm, **P2a** at 551 nm and **P3a** at 345 nm. *In situ* absorbance spectrum in Milli-Q under illumination conditions of D) **P1a** illuminated with 530 nm light, E) **P2a** illuminated with 365 nm light and F) **P3a** illuminated with 365 nm light. [Polymer] = 1 mg mL^{-1}.

remains highly stable, retaining 91% of its absorbance at 432 nm over 15 h (Fig. 1B). Reversible *Z*–*E* isomerization is efficiently induced by 450 nm light, enabling precise control (Fig. S87C). Over three switching cycles, **P3** maintains 99% of its absorbance, indicating minimal fatigue (Fig. S87D). Polymers **P4** and **P5**, also functionalized with AAIP, exhibit analogous photophysical behavior (see Fig. S90–S92). Importantly, **P4** shows switching within one minute under 25-fold reduced light intensity, supporting their suitability for biologically relevant applications (Fig. S91C).

Together, these results show that while all photoswitches undergo light-induced isomerization when incorporated into SCPNs, their stability and reversibility differ markedly. The pronounced thermal relaxation observed for DASA and SP likely arises from the dynamic, loosely packed nature of SCPNs, which resemble intrinsically disordered proteins rather than compact hydrophobic domains.[55] This structural softness may limit the shielding of the photoswitch from water, in contrast to more rigid assemblies such as polymersomes, where hydrophobic confinement stabilizes apolar isomers.[30]

Given the requirements of this study, *i.e.* precise control over photoisomerization and long term stability on timescales relevant for conformational and biological experiments, we focus subsequent investigations on AAIP functionalized SCPNs.

Global conformations in AAIP-based polymers

With the development of SCPNs functionalized with the highly controllable and stable photoswitch AAIP, our aim is to investigate their conformational properties in aqueous solution. Previous studies demonstrated the profound influence of side-graft composition on particle conformation, influencing parameters such as size, shape, compactness and aggregation propensity.[41,50] Here, we introduce a positively charged side-graft and evaluate how this modification affects the collapsed conformation of the resulting SCPNs. We determine whether our newly designed SCPNs remain collapsed in water and characterize their compactness, size and shape. To this end, we employ small-angle X-ray scattering (SAXS), dynamic light scattering (DLS) and both proton- and diffusion-ordered spectroscopy- (DOSY) NMR spectroscopy.[56]

Polymers **P3a–P5a** were first evaluated in Milli-Q in their pristine *E*-isomer using SAXS. Collapse of the SCPNs was assessed using Kratky analysis (Fig. 2A). All polymers displayed a peak in the Kratky plot, consistent with a collapsed structure. **P4a** and **P5a** exhibited a sharper peak than **P3a**, indicating a more pronounced collapsed and compact structure. These observations align with previous results where Jeffamine M1000-based SCPNs resemble an intrinsically disordered protein in Kratky analysis and glucose-based SCPNs obtain a more collapsed conformation.[50,55] The control polymer **P9**, containing 100% glucose side-grafts, showed an increasing, featureless Kratky plot, characteristic of an unfolded conformation (Fig. S93). These finding are corroborated by ^{1}H-NMR spectroscopy. Hydrophobic collapse was assessed by comparing spectra for **P3a** in $CDCl_3$ and D_2O and **P4a** and **P5a** in DMSO-d_6 and D_2O. In organic solvents, all side-graft signals were well resolved for **P3a–P5a**. In contrast, in D_2O, significant peak broadening and signal reduction was observed for *n*-dodecyl and AAIP side-grafts, consistent with reduced T2 relaxation times. This effect is indicative of confinement of the protons of interest due to particle formation (Fig. S57, S58, S62, S63, S68 and S69).[57] Furthermore, DOSY-NMR shows that **P4a** and **P5a** diffuse more rapidly than the non-collapsed **P9**, confirming their collapsed structure (Table S1).

Having confirmed their collapsed nature, we next studied the size of the SCPNs. The radius of gyration (R_G) was determined using Guinier analysis. For **P3a–P5a**, the extracted R_G values fall within the same order of magnitude, ranging from 5–6 nm (Table 2). The R_G of 5.6 nm of **P3a** is consistent with the SCPN size range.[50] Given the much smaller size of polymers **P4a** and **P5a**, smaller R_G values were expected for a single chain nanoparticle. Furthermore,

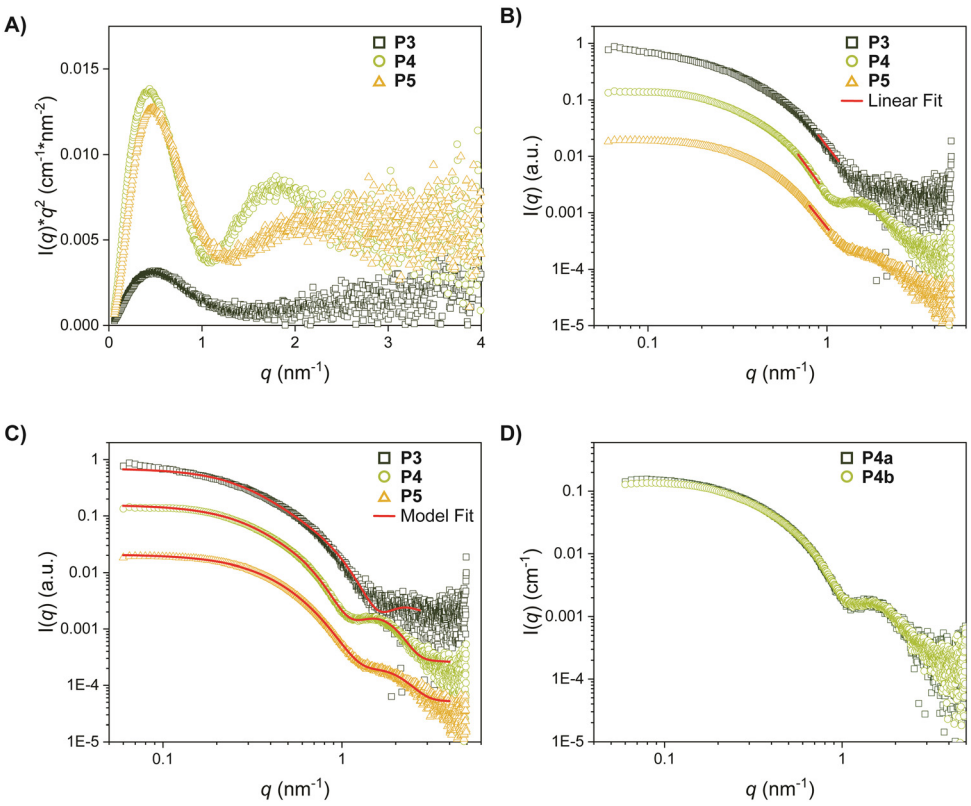

Fig. 2 SAXS analysis of **P3–P5** in Milli-Q. A) Kratky plots, B) fractal dimension analysis of **P3a–P5a** in water performed at high *q* power law regimes. SAXS curves are off-set for clarity. C) SAXS curves of **P3a–P5a** in water and the form factor fit of flexible cylinder for **P3a** and core–shell ellipsoid for **P4a** and **P5a**. [**P3**] = 2.5 mg mL^{-1}, [**P4–P5**] = 2 mg mL^{-1}. SAXS curves are off-set for clarity. D) SAXS curves of P4 in water pristine (**P4a**) and after illumination with 365 nm light (**P4b**). [**P4**] = 1 mg mL^{-1}.

Table 2 R_G from the Guinier analysis, R_H from DLS analysis, fractal dimension analysis in the high q region (D_{high}) and the Py-ratios for **P3**–**P5**

Polymer	R_G[a] (nm)	R_H (nm)	D_{high}[a]	Py-*E*	Py-*Z*
P3	5.6 ± 0.3	6.5[b]	4.0 ± 0.1	0.8	1.5
P4	5.9 ± 0.4	5.3 ± 0.6[c]	4.5 ± 0.1	1.4	2.0
P5	5.0 ± 0.4	6.3 ± 0.6[d]	4.1 ± 0.1	1.2	1.7

[a] Averaged over all measured concentrations. [b] Result of one measurement. [c] Average of 4 measurements. [d] Average of 2 measurements.

previous MD simulations revealed that the structure of a multichain aggregate of 3 chains agrees better with the experimental SAXS data for glucose-based polymeric nanoparticles.[50] Therefore, we hypothesize here that **P4a** and **P5a** consist out of small amphiphilic polymeric nanoparticles comprising multiple chains. Additionally, **P3** also contains a small fraction of larger aggregates as evident by the upturn at low q-range in the Guinier plot (Fig. S94). From DLS analysis, the hydrodynamic radii were obtained. Here, **P3a** demonstrates a monomodal size distribution with a R_H = 6.5 nm. **P4a** and **P5a** form particles of R_H = 5.3 ± 0.6 nm and R_H = 6.3 ± 0.6 nm respectively. The ratio R_G/R_H, also called the shape factor ρ, provides information on the particle morphology. For all systems, ρ exceeds 0.77, which is inconsistent with a homogeneous solid sphere ($\rho \approx 0.775$) and suggests an elongated or anisotropic conformation. All samples exhibit smooth particle surfaces, as evidenced by the high q-range of the SAXS profiles, which yield fractal dimensions (D_{high}) close to 4. In contrast, control polymer **P9** has a fractal dimension of 1.7, exactly in agreement with the value for a well-solvated polymer with excluded volume (Fig. 2B, Tables 2 and S3).

Further insight into the shape of the SCPNs is obtained using form factor fitting. From the different shapes of the 1D SAXS curves of **P3a–P5a**, we can immediately conclude that all designed SCPNs have a different structure (Fig. 2C). For **P3a** a smooth curve with little features is obtained, in line with previous Jeffamine M1000 polymers studied in our group and suggests a worm-like structure. We could indeed successfully fit the curve of **P3a** with a flexible cylinder model, obtaining a length of 42 nm and radius of 2.2 nm. The fitted length is significantly reduced compared to the theoretical contour length of 85 nm, indicating a significant collapse of the structure (Table S4). This is somewhat unexpected for a Jeffamine based polymer, but in line with the small R_G obtained from the Guinier analysis and the small diffusion coefficient in DOSY. **P4a** and **P5a** display a clear plateau at low q with an oscillatory feature at q = 1–2 nm^{-1}. This feature indicates the presence of two domains in the polymer structure and could be interpreted as a core–shell structure. For **P5a** the oscillatory feature is smoothened out, suggesting a less defined core–shell structure. Given these characteristics, we fit **P4a** and **P5a** with a core–shell ellipsoid model (Table S5). For both polymers a prolate structure is obtained with a minor radius of 2.8 and 2.3 nm for **P4a** and **P5a** respectively and an aspect ratio of 4.9 and 2.5 nm respectively, suggesting that **P4a** adopts a more pronounced prolate structure than **P5a**. For all fits the low χ^2 value is indicative of a good fit and the anisotropy of the form factor models is in line with the asymmetry observed in the pair distance distribution functions for all polymers (Fig. S95).

Influence of AAIP side-graft on SCPN conformation. With the general structure of the photoresponsive SCPNs elucidated, we next examined the extent to which the photoswitch side-graft influences their overall conformation. To this end, SAXS analysis was also performed on the precursor polymers, *i.e.* the amphiphilic random heterograft polymers with only the click-handle present, **P6** and **P7**. For **P3**, an analogous amphiphilic polymer **P8** with 20 mol% *n*-dodecyl side-grafts and 80 mol% Jeffamine M1000 side-grafts served as reference. Interestingly, the overall shape of the 1D SAXS curves remains unchanged upon introducing the AAIP moiety for all polymers studied (Fig. S96). For **P3**, previous work has shown that the SCPN conformation is primarily governed by the Jeffamine M1000 side-grafts, and these results are consistent with that.[50] In the case of **P4** and **P5**, the collapsed structure appears to be dictated mainly by the proportion of *n*-dodecylamine side-grafts on the polymer backbone. Addition of the photoswitch unit does not alter the conformation, even though the AAIP moiety includes a C11 alkyl linker that might have been expected to introduce further hydrophobic interactions. These findings are also consistent with DOSY-NMR measurements, which likewise reveal no structural differences (Table S1).

Influence of photoisomerization upon SCPN conformation. Next, we investigated whether photoisomerization of the AAIP photoswitch affects the global conformation of the SCPNs. As outlined above, the *E–Z* isomerization is associated with a change in dipole moment, and we therefore aimed to determine whether this molecular switch perturbs the collapsed structure of these inherently dynamic SCPNs. For this purpose, SCPN solutions were irradiated with 365 nm light and subsequently analysed by SAXS.

Curiously, photoisomerization does not induce any change in global conformation for any of the photoresponsive systems studied (Fig. 2D and S97). The SAXS profiles of the *E* and *Z* rich SCPNs are fully overlapping, demonstrating that the overall particle morphology remains unchanged. DOSY-NMR measurements corroborate this observation, as no significant differences in diffusion behavior are detected between the two isomers (Table S1).

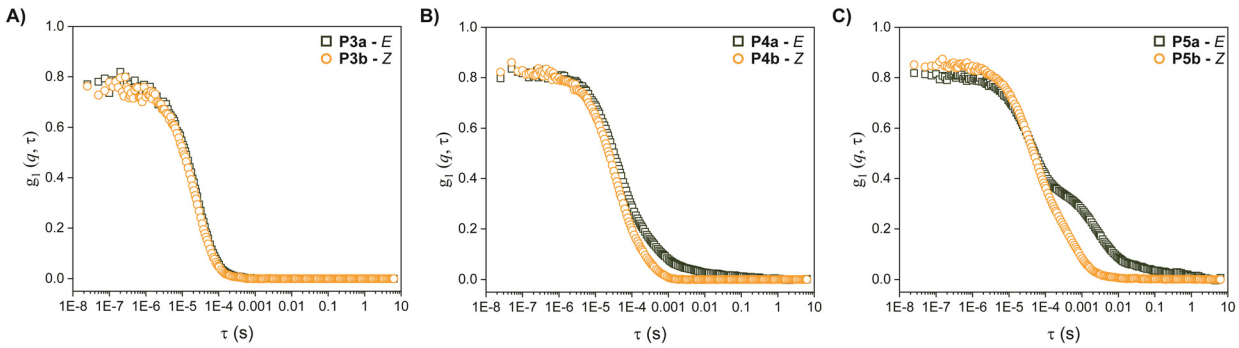

Fig. 3 Dynamic light scattering correlogram curves for A) **P3**, B) **P4** and C) **P5** at 90° in Milli-Q before (**P3a**–**P5a**) and after illumination with 365 nm (**P3b**–**P5b**). [**P3**] = 1 mg mL^{-1}, [**P4**–**P5**] = 0.3 mg mL^{-1}.

Interestingly, however, more subtle microstructural effects appear to be present. In dynamic light scattering, **P4b** shows a slight change in the correlogram upon irradiation, while **P5b** exhibits a pronounced change; in contrast, **P3b** remains unaffected (Fig. 3). Consistent with this, the ^{1}H-NMR spectrum of **P5b** displays increasingly sharp proton peaks after illumination (Fig. S72). Although these observations are indirect and not highly specific, they might point to a reorganization within the polymer microenvironment upon photoisomerization despite the overall conformation remaining constant.

Influence of photoisomerization on SCPN microenvironment. As the global conformation of the polymeric nanoparticles does not change, we decided to also investigate the polymer microenvironment using a polarity probe. A well-known technique to detect the formation of hydrophobic compartments, is the addition of a fluorescent probe such as pyrene. Pyrene has distinct vibronic bands at 373 and 383 nm in its fluorescence spectrum, whose ratio (Py-ratio) is indicative of the polarity of the environment. A higher ratio indicates a more polar environment. **P3a**–**P5a** all demonstrate a reduced Py-ratio (0.8–1.2) compared to pure water (1.7), indicating the presence of hydrophobic domains (Table 2, Fig. S98 and S99). Interestingly, upon photoisomerization, for all three polymers **P3b**–**P5b** a significant increase to higher Py-ratios is observed, demonstrating that pyrene feels a more polar environment, suggesting less well-defined hydrophobic compartments present (Table 2, Fig. S99 and S100). A control experiment probing molecularly dissolved AAIP in water shows no change in Py-ratio upon photoisomerization, suggesting that the observed effect originates from photoinduced modifications in the polymeric microstructure (Fig. S101). This increase in polarity aligns with the NMR results where the increasingly sharp proton peaks upon illumination indicate increased proton mobility (Fig. S72). These results demonstrate that despite the presence of a permanent positive charge, AAIP photoswitches can affect the local polarity of SCPNs.

To summarize, we obtain control over the microenvironment in the SCPNs while maintaining the global conformation. This phenomenon is commonly observed in literature as well. Voets *et al.* demonstrated that the addition of DMSO to lysozymes disrupts the internal microstructure before a global denaturation was observed in the neutron scattering signal.[58] Similarly, the work of Bruns and coworkers employing DASA photoswitches in polymersomes membranes demonstrates that the change in permeability of the membrane is not accompanied by a change in membrane morphology.[30]

Exploring biocompatibility

Finally, the potential for biological applications was evaluated by performing an exploratory cytotoxicity assay on HeLa cells. Although positive charges are known to facilitate cytosolic delivery of SCPNs, an excessive cationic character can also induce premature cell death.[59] Both **P4** and **P5** were introduced to the cells in their *E* and *Z* isomeric forms. The *Z*-isomers (**P4b** and **P5b**) were generated by illuminating the polymers prior to cell exposure, ensuring that light treatment itself did not influence cell viability and allowing us to isolate the effect of isomerization. Across all measurements, no difference in cell viability was observed between the *E* and *Z* forms, indicating that isomerization does not affect cytotoxicity. In contrast, clear differences emerged between **P4** and **P5** (Fig. 4). For **P4a**, cell viability remained excellent across all tested concentrations (0.05–1 mg mL^{-1}). **P5a**, however, displayed significant cytotoxicity, reducing viability to 63% already at 0.1 mg mL^{-1}. Because **P5a** contains twice the amount of AAIP compared to **P4a**, the increased toxicity initially appears linked to its higher positive charge density. However, even when normalizing for total charge, **P5a** remains substantially more cytotoxic. For instance, at 0.5 mg mL^{-1} **P4a**, the solution contains ~60 μM AAIP while maintaining 99% viability, whereas at only 0.21 mg mL^{-1} **P5a**, corresponding to ~48 μM AAIP, cell viability drops to 38% (Fig. S102). These results suggest that cytotoxicity cannot be attributed solely to overall cationic charge concentration. In **P5a**, a larger number of positive charges is concentrated on a single polymer chain, creating a locally high charge density that may induce multivalent-like effects.

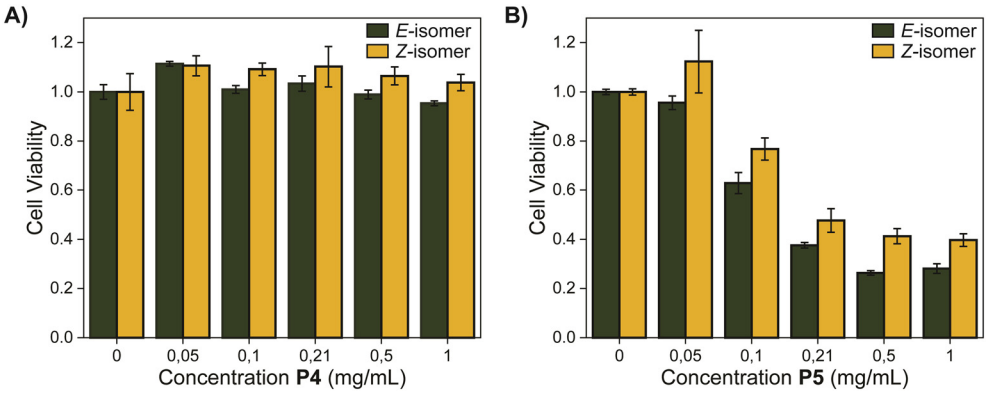

Fig. 4 CCK-8 cytotoxicity assay of HeLa cells incubated for 24 h with A) **P4** and B) **P5** at various concentrations. Error bars represent the standard deviation of 3 measurements.

Furthermore, structural differences between the two SCPNs likely influence how the charges are presented at the nanoparticle-cell interface and might lead to a different biological interaction. Prior work from Stenzel and coworkers has shown that even subtle variations in SCPN composition can lead to pronounced differences in biological behaviour, due to their strong impact on properties such as compactness and solubility.[60] This trend is also reflected in our SAXS analysis: although **P4a** and **P5a** differ only slightly in composition, their structural signatures are distinct (Fig. 2C). These variations likely contribute to the divergent biological responses observed.

Overall, while both polymers share similar chemical building blocks, their differing nanoscale structures appear to play a key role in determining cytotoxicity. Further in depth cellular studies are underway to clarify the precise mechanisms governing their biological interactions.

Conclusions

In conclusion, we have demonstrated the successful development of photoresponsive SCPNs by incorporation of three different photoswitches; DASA, SP and AAIP. Thermal stability limitations of DASA and SP hampered the effective use of these photoswitches, leading to the conformational exploration of AAIP functionalized SCPNs. SAXS analysis confirmed that differences in hydrophilic side-graft chemistry strongly influence particle conformation: **P3**, bearing Jeffamine M1000 side-grafts, forms flexible worm-like cylindrical particles, whereas **P4** and **P5**, equipped with glucose-based grafts, adopt core–shell ellipsoidal structures. Importantly, at photoswitch loadings up to and below 10 mol%, the global particle conformation remains unaffected by the introduction of a positively charged side-graft photoswitch. Furthermore, photoisomerization does not disrupt the global SCPN morphology.

While the macroscopic conformation is preserved, we achieve clear control over the particle microstructure. The *E*–*Z* isomerization of the AAIP directs the local environment toward increased polarity as reflected by the elevated Py-ratio. This decoupling of global structure from microstructural responsiveness represents a meaningful design handle for tuning internal organization.

Simultaneously, this study underscores how small molecular design changes can produce significant and largely unpredictable biological responses – illustrated by the notably higher cytotoxicity of **P5** compared to **P4**. These outcomes highlight the difficulty of navigating the SCPN design space, where side-graft character and composition play a central but complex role in governing structure-interaction relationships.

Ultimately, our findings show that microstructure can be selectively modulated without altering overall particle morphology, offering opportunities in applications such as catalysis, where substrate accessibility and catalyst performance are highly sensitive to SCPN microstructure. As previously demonstrated, compartmentalized SCPNs can selectively take up hydrophobic substrates due to their persistent hydrophobic interior.[61] The present system could work complementary as the switchable polarity of the microstructure could allow the uptake of more polar substrates, all while maintaining the global structural integrity.

Author contributions

The manuscript was written through contributions of all authors. All authors have given approval to the final version of the manuscript.

Conflicts of interest

There are no conflicts of interest to declare.

Data availability

Supplementary information (SI): synthetic procedures for photoswitches and polymers. Full characterisation of photoswitches and polymers. Sample preparation procedures. Cell study procedures. Additional UV-absorbance measurements. Additional SAXS measurements. Additional

DLS measurements. Additional pyrene fluorescence measurements. See DOI: https://doi.org/10.1039/d6me00057f.

Acknowledgements

This project has received funding from The Dutch Ministry of Education, Culture and Science, Netherlands (NWO Gravitation program 024.005.020: Interactive Polymer Materials) and the TU/e. We thank the staff of the ESRF and EMBL Grenoble for assistance and support in using beamline BM29 under proposal number MX-2671 and MX-2677. The authors thank Dr. Marcel van Genderen and Prof. Ilja Voets for providing feedback on NMR and SAXS results.

Notes and references

1 A. Balcerak-Woźniak, M. Dzwonkowska-Zarzycka and J. Kabatc-Borcz, A Comprehensive Review of Stimuli-Responsive Smart Polymer Materials—Recent Advances and Future Perspectives, *Materials*, 2024, **17**, 4255.
2 D. Mariottini, D. Del Giudice, G. Ercolani, S. Di Stefano and F. Ricci, Dissipative operation of pH-responsive DNA-based nanodevices, *Chem. Sci.*, 2021, **12**, 11735–11739.
3 J. Singh and P. Nayak, pH-responsive polymers for drug delivery: Trends and opportunities, *J. Polym. Sci.*, 2023, **61**, 2828–2850.
4 M. Nakamura, S. N. Nishimura, N. Higashi and T. Koga, Thermo-responsive injectable hydrogels from linear and star-shaped block copolymers composed of amino acid-derived vinyl polymer and poly(ethylene glycol) for biomedical applications, *Mater. Adv.*, 2024, **5**, 665–674.
5 C. Zhao, Z. Ma and X. X. Zhu, Rational design of thermoresponsive polymers in aqueous solutions: A thermodynamics map, *Prog. Polym. Sci.*, 2019, **90**, 269–291.
6 R. Patra, S. Halder, R. Saha, K. Jana and K. Sarkar, Highly Efficient Photoswitchable Smart Polymeric Nanovehicle for Gene and Anticancer Drug Delivery in Triple-Negative Breast Cancer, *ACS Biomater. Sci. Eng.*, 2024, **10**, 2299–2323.
7 K. Y. Zhang, S. Liu, Q. Zhao and W. Huang, Stimuli–responsive metallopolymers, *Coord. Chem. Rev.*, 2016, **319**, 180–195.
8 S. Xian, Y. Xiang, K. Mitrová, J. Jiráček and M. J. Webber, Diboronate-Modified Hyaluronic Acid for Glucose-Responsive Insulin Delivery, *Biomacromolecules*, 2025, **26**, 2700–2707.
9 R. Ma and L. Shi, Phenylboronic acid-based glucose-responsive polymeric nanoparticles: synthesis and applications in drug delivery, *Polym. Chem.*, 2014, **5**, 1503–1518.
10 J. J. B. van der Tol, T. A. P. Engels, R. Cardinael, G. Vantomme, E. W. Meijer and F. Eisenreich, Photoswitchable Liquid-to-Solid Transition of Azobenzene-Decorated Polysiloxanes, *Adv. Funct. Mater.*, 2023, **33**, 2301246.
11 M. Di Martino, L. Sessa, R. Diana, S. Piotto and S. Concilio, Recent Progress in Photoresponsive Biomaterials, *Molecules*, 2023, **28**, 3712.
12 H. M. D. Bandara and S. C. Burdette, Photoisomerization in different classes of azobenzene, *Chem. Soc. Rev.*, 2012, **41**, 1809–1825.
13 R. Klajn, Spiropyran-based dynamic materials, *Chem. Soc. Rev.*, 2013, **43**, 148–184.
14 M. Clerc, S. Sandlass, O. Rifaie-Graham, J. A. Peterson, N. Brun, J. Read de Alaniz and L. F. Boesel, Visible light-responsive materials: the (photo)chemistry and applications of donor–acceptor Stenhouse adducts in polymer science, *Chem. Soc. Rev.*, 2023, **52**, 8245–8294.
15 F. A. Jerca, V. V. Jerca and R. Hoogenboom, Advances and opportunities in the exciting world of azobenzenes, *Nat. Rev. Chem.*, 2021, **6**, 51–69.
16 Z. Y. Zhang, D. Dong, T. Bösking, T. Dang, C. Liu, W. Sun, M. Xie, S. Hecht and T. Li, Solar Azo-Switches for Effective E→Z Photoisomerization by Sunlight, *Angew. Chem., Int. Ed.*, 2024, **63**, e202404528.
17 G. S. Hartley and R. J. W. Le Fèvre, 119. The dipole moments of cis- and trans-azobenzenes and of some related compounds, *J. Chem. Soc.*, 1939, 531–535.
18 A. Mukherjee, M. D. Seyfried and B. J. Ravoo, Azoheteroarene and Diazocine Molecular Photoswitches: Self-Assembly, Responsive Materials and Photopharmacology, *Angew. Chem., Int. Ed.*, 2023, **62**, e202304437.
19 C. E. Weston, R. D. Richardson, P. R. Haycock, A. J. P. White and M. J. Fuchter, Arylazopyrazoles: Azoheteroarene photoswitches offering quantitative isomerization and long thermal half-lives, *J. Am. Chem. Soc.*, 2014, **136**, 11878–11881.
20 A. K. Gaur, D. Gupta, A. Mahadevan, P. Kumar, H. Kumar, D. N. Nampoothiry, N. Kaur, S. K. Thakur, S. Singh, T. Slanina and S. Venkataramani, Bistable Aryl Azopyrazolium Ionic Photoswitches in Water, *J. Am. Chem. Soc.*, 2023, **145**, 10584–10594.
21 K. Manna, D. Dolai, S. Ghosh, S. Samanta, S. Dey and S. Pal, Photoinduced Ultrafast Shape-Changing Self-Assembled Arylazopyrazole-Based Polymeric Micelles, *Macromolecules*, 2024, **57**, 8445–8458.
22 R. Steinbrecher, F. Lehmann, R. Nedielkov, T. Klamroth, H. Möller, A. Taubert, D. Hinderberger, P. Müller-Buschbaum, C. M. Papadakis and A. Laschewsky, Toward Fully Photoresponsive Amphiphilic Polymers via Azopyrazole-Functionalized Polyacrylamides, *Macromolecules*, 2025, **58**, 11088–11098.
23 G. Berkovic, V. Krongauz and V. Weiss, Spiropyrans and Spirooxazines for Memories and Switches, *Chem. Rev.*, 2000, **100**, 1741–1753.
24 C. Li, A. Iscen, L. C. Palmer, G. C. Schatz and S. I. Stupp, Light-Driven Expansion of Spiropyran Hydrogels, *J. Am. Chem. Soc.*, 2020, **142**, 8447–8453.
25 R. Tong, H. D. Hemmati, R. Langer and D. S. Kohane, Photoswitchable Nanoparticles for Triggered Tissue Penetration and Drug Delivery, *J. Am. Chem. Soc.*, 2012, **134**, 8848–8855.

26 S. Son, E. Shin and B. S. Kim, Light-Responsive Micelles of Spiropyran Initiated Hyperbranched Polyglycerol for Smart Drug Delivery, *Biomacromolecules*, 2014, **15**, 628–634.

27 S. Helmy, F. A. Leibfarth, S. Oh, J. E. Poelma, C. E. Hawker and J. Read de Alaniz, Photoswitching using visible light: A new class of organic photochromic molecules, *J. Am. Chem. Soc.*, 2014, **136**, 8169–8172.

28 M. M. Lerch, W. Szymański and B. L. Feringa, The (photo)chemistry of Stenhouse photoswitches: guiding principles and system design, *Chem. Soc. Rev.*, 2018, **47**, 1910–1937.

29 S. O. Poelma, S. S. Oh, S. Helmy, A. S. Knight, G. L. Burnett, T. Soh, C. E. Hawker and J. Read de Alaniz, Controlled drug release to cancer cells from modular one-photon visible light-responsive micellar system, *Chem. Commun.*, 2016, **52**, 10525–10528.

30 O. Rifaie-Graham, S. Ulrich, N. F. B. Galensowske, S. Balog, M. Chami, D. Rentsch, J. R. Hemmer, J. Read de Alaniz, L. F. Boesel and N. Bruns, Wavelength-Selective Light-Responsive DASA-Functionalized Polymersome Nanoreactors Omar, *J. Am. Chem. Soc.*, 2018, **140**, 8027–8036.

31 A. Latorre-Sanchez and J. A. Pomposo, A simple, fast and highly sensitive colorimetric detection of zein in aqueous ethanol via zein–pyridine–gold interactions, *Chem. Commun.*, 2015, **51**, 15736–15738.

32 C.-C. Cheng, S.-Y. Huang, W.-L. Fan, A.-W. Lee, C.-W. Chiu, D.-J. Lee and J.-Y. Lai, Water-Soluble Single-Chain Polymeric Nanoparticles for Highly Selective Cancer Chemotherapy, *ACS Appl. Polym. Mater.*, 2020, **3**, 474–484.

33 A. P. P. Kröger and J. M. J. Paulusse, Single-chain polymer nanoparticles in controlled drug delivery and targeted imaging, *J. Controlled Release*, 2018, **286**, 326–347.

34 F. Eisenreich and A. R. A. Palmans, Direct C–H Trifluoromethylation of (Hetero)Arenes in Water Enabled by Organic Photoredox-Active Amphiphilic Nanoparticles, *Chem. – Eur. J.*, 2022, **28**, e202201322.

35 D. Arena, E. Verde-Sesto, I. Rivilla and J. A. Pomposo, Artificial Photosynthases: Single-Chain Nanoparticles with Manifold Visible-Light Photocatalytic Activity for Challenging "in Water" Organic Reactions, *J. Am. Chem. Soc.*, 2024, **146**, 14397–14403.

36 L. de Jonge, I. Hazenberg, H. Singh, A. P. Prakasham and A. R. A. Palmans, Consequences of encapsulated vs. covalently attached Pd-NHC amphiphilic polymeric nanocatalysts in bioorthogonal catalysis, *Chem. Commun.*, 2026, **62**, 4094–4098.

37 S. Wijker and A. R. A. Palmans, Protein-Inspired Control over Synthetic Polymer Folding for Structured Functional Nanoparticles in Water, *ChemPlusChem*, 2023, **88**, e202300260.

38 G. M. ter Huurne, A. R. A. Palmans and E. W. Meijer, Supramolecular single-chain polymeric nanoparticles, *CCS Chem.*, 2019, **1**, 64–82.

39 A. P. P. Kröger, M. I. Komil, N. M. Hamelmann, A. Juan, M. H. Stenzel and J. M. J. Paulusse, Glucose Single-Chain Polymer Nanoparticles for Cellular Targeting, *ACS Macro Lett.*, 2018, **8**, 95–101.

40 Y. Abdouni, G. M. ter Huurne, G. Yilmaz, A. Monaco, C. Redondo-Gómez, E. W. Meijer, A. R. A. Palmans and C. R. Becer, Self-Assembled Multi- and Single-Chain Glyconanoparticles and Their Lectin Recognition, *Biomacromolecules*, 2020, **22**, 661–670.

41 G. M. ter Huurne, L. N. J. de Windt, Y. Liu, E. W. Meijer, I. K. Voets and A. R. A. Palmans, Improving the Folding of Supramolecular Copolymers by Controlling the Assembly Pathway Complexity, *Macromolecules*, 2017, **50**, 8562–8569.

42 Z. Cui, H. Cao, Y. Ding, P. Gao, X. Lu and Y. Cai, Compartmentalization of an ABC triblock copolymer single-chain nanoparticle via coordination-driven orthogonal self-assembly, *Polym. Chem.*, 2017, **8**, 3755–3763.

43 Y. Bai, X. Feng, H. Xing, Y. Xu, B. K. Kim, N. Baig, T. Zhou, A. A. Gewirth, Y. Lu, E. Oldfield and S. C. Zimmerman, A Highly Efficient Single-Chain Metal–Organic Nanoparticle Catalyst for Alkyne–Azide "Click" Reactions in Water and in Cells, *J. Am. Chem. Soc.*, 2016, **138**, 11077–11080.

44 T. Terashima, T. Sugita, K. Fukae and M. Sawamoto, Synthesis and Single-Chain Folding of Amphiphilic Random Copolymers in Water, *Macromolecules*, 2014, **47**, 589–600.

45 S. Wijker, L. Deng, F. Eisenreich, I. K. Voets and A. R. A. Palmans, En Route to Stabilized Compact Conformations of Single-Chain Polymeric Nanoparticles in Complex Media, *Macromolecules*, 2022, **55**, 6220–6230.

46 S. Wijker, R. Monnink, L. Rijnders, L. Deng and A. R. A. Palmans, Simultaneously controlling conformational and operational stability of single-chain polymeric nanoparticles in complex media, *Chem. Commun.*, 2023, **59**, 5407–5410.

47 A. E. Izuagbe, B. T. Tuten, C. Barner-Kowollik, A. E. Izuagbe and P. W. Roesky, Light-driven folding of single polymer chains via metal-complexation, *Polym. Chem.*, 2024, **15**, 1955–1961.

48 L. Deng, A. R. Olea, A. Ortiz-Perez, B. Sun, J. Wang, S. Pujals, A. R. A. Palmans and L. Albertazzi, Imaging Diffusion and Stability of Single-Chain Polymeric Nanoparticles in a Multi-Gel Tumor-on-a-Chip Microfluidic Device, *Small Methods*, 2024, **8**, 2301072.

49 Y. Liu, T. Pauloehrl, S. I. Presolski, L. Albertazzi, A. R. A. Palmans and E. W. Meijer, Modular Synthetic Platform for the Construction of Functional Single-Chain Polymeric Nanoparticles: From Aqueous Catalysis to Photosensitization, *J. Am. Chem. Soc.*, 2015, **137**, 13096–13106.

50 S. Wijker, D. Dellemme, L. Deng, B. Fehér, I. K. Voets, M. Surin and A. R. A. Palmans, Revealing the Folding of Single-Chain Polymeric Nanoparticles at the Atomistic Scale by Combining Computational Modeling and X-ray Scattering, *ACS Macro Lett.*, 2025, **14**, 428–433.

51 T. J. Neal, A. J. Parnell, S. M. King, D. L. Beattie, M. W. Murray, N. S. J. Williams, S. N. Emmett, S. P. Armes, S. G. Spain and O. O. Mykhaylyk, Control of Particle Size in the Self-Assembly of Amphiphilic Statistical Copolymers, *Macromolecules*, 2021, **54**, 1425–1440.

52 Y. Vo, R. Raveendran, C. Cao, L. Tian, R. Y. Lai and M. H. Stenzel, Tadpole-like cationic single-chain nanoparticles display high cellular uptake, *J. Mater. Chem. B*, 2024, **12**, 12627–12640.

53 A. Sathyan, E. Archontakis, A. J. H. Spiering, L. Albertazzi and A. R. A. Palmans, Effect of Particle Heterogeneity in Catalytic Copper-Containing Single-Chain Polymeric Nanoparticles Revealed by Single-Particle Kinetics, *Molecules*, 2024, **29**, 1850.

54 F. G. Blandón-Cumbreras, M. Jurtík, A. Závodná, P. Janovský, M. Rouchal, R. Vícha and U. Pischel, Reversible Photoswitching of Donor–Acceptor Stenhouse Adducts in Water, *J. Am. Chem. Soc.*, 2025, **148**, 130–134.

55 J. A. Pomposo, I. Perez-Baena, F. Lo Verso, A. J. Moreno, A. Arbe and J. Colmenero, How Far Are Single-Chain Polymer Nanoparticles in Solution from the Globular State?, *ACS Macro Lett.*, 2014, **3**, 767–772.

56 B. D. Monnery, V. V. Jerca, R. Hoogenboom and T. Swift, Polymer conformation determination by NMR spectroscopy: comparative diffusion ordered 1H-NMR spectroscopy of poly(2-ethyl-2-oxazoline)s and poly(ethylene glycol) in D2O, *Polym. Chem.*, 2024, **15**, 3077–3085.

57 S. Liao, L. Wei, L. A. Abriata and F. Stellacci, Control and Characterization of the Compactness of Single-Chain Nanoparticles, *Macromolecules*, 2021, **54**, 11459–11467.

58 I. K. Voets, W. A. Cruz, C. Moitzi, P. Lindner, E. P. G. Arêas and P. Schurtenberger, DMSO-Induced Denaturation of Hen Egg White Lysozyme, *J. Phys. Chem. B*, 2010, **114**, 11875–11883.

59 N. M. Hamelmann, J. W. D. Paats and J. M. J. Paulusse, Cytosolic Delivery of Single-Chain Polymer Nanoparticles, *ACS Macro Lett.*, 2021, **10**, 1443–1449.

60 Y. Vo, M. D. Nothling, R. Raveendran, C. Cao and M. H. Stenzel, Effects of Drug Conjugation on the Biological Activity of Single-Chain Nanoparticles, *Biomacromolecules*, 2024, **25**, 675–689.

61 M. Artar, E. R. J. Souren, T. Terashima, E. W. Meijer and A. R. A. Palmans, Single Chain Polymeric Nanoparticles as Selective Hydrophobic Reaction Spaces in Water, *ACS Macro Lett.*, 2015, **4**, 1099–1103.